accepted for publication in 2020 IEEE International Instrumentation & Measurement Technology Conference (I2MTC)

# Scalable Retrofit Angular Position Sensor System

Harald Gietler, Christian Stetco and Hubert Zangl
Institute of Smart Systems Technologies, Sensors and Actuators
University of Klagenfurt
Universitätsstraße 65-67, 9020 Klagenfurt
Email: harald.gietler@aau.at

***Abstract*—This article presents an angular position measurement system, designed to match the needs of the ever growing field of robotics and automation. Often existing systems should be equipped with sensors to enable autonomous acting. The presented sensor front-end is comprised of a single transmitter and two receiver coils. The mutual inductance between transmitter and receiver coils is spatially modulated using conductive objects. The resulting measurements are the basis for the absolute angle estimation. Here, the entire geometry requires $270^\circ$ which makes it retrofittable to existing systems. The coil design is based on Finite Element Method simulation. The simulation framework allows for robust design with respect to detrimental effects such as tilt between the coils and modulating objects. Additionally, the sensor front-end is scalable in size to match different devices in automation. The underlying physical principle guarantees for robustness with respect to many detrimental effects such as moisture, bad illumination or oil contamination. Access to the data is provided using CAN bus as well as Bluetooth wireless connection. The applicability of the sensor system is showcased on the example of an industrial log-grasping crane.**

***Index Terms*—Computational electromagnetics, Magnetic field measurement, Rotation measurement.**

## I. Introduction

The ever increasing number of autonomous systems employed in various industrial fields pushes the demand of robust and reliable sensors. Autonomous systems need precise information about their internal states to fulfill tasks such as picking and placing objects. Therefore, accurate and robust sensors which endure harsh conditions over a long period of time are required. Typical detrimental effects in the industrial field are moisture, oil, mud as well as bad illumination and vibration. Used sensors are not only required to be unaffected by those circumstances but should also be contact-free in order to sustain their functionality over a long period of time. This work focuses on sensors which are able to monitor the angular displacement of rotating shafts. They are required to provide absolute angular position information over a $360^\circ$ range. Sensors which can be mounted in a retrofit fashion without disassembling the device are of special interests, due to their extended applicability.

Various angular position sensor types based on different physical principles are readily available. Sensors based on capacitive principles rely on the change of geometry or permittivity [1]. It is advantageous, that they are contact-free and their design and implementation is cost effective. Although, such sensors suffer from harsh environmental conditions due to their underlying physical principles, e.g. moisture affects the permittivity. Another common form of contact-free angular position sensors are based on optical principles. Here, a light beam is shone through or onto a grating and the resulting light is measured by a photo detector. The grating provides a position encoding. Optical systems can achieve very high resolution and accuracy, but require direct line of sight [2]. Often, in open industrial environments it can not be guaranteed that the respective area is free of dirt and dust, which may decrease the sensor performance.

The magnetic principle is an alternative which can be very robust. Commonly, sensors such as anisotropic magnetoresistive sensors (AMR, e.g. [3]), giant magnetoresistive sensors (GMR, e.g. [4]), tunneling magnetoresistive sensors (TMR, e.g. [5]) and Hall effect sensors (e.g. [6]) are used. This paper presents an inductive sensor comprised of a single transmitting coil and two receiving coils. A time-varying current, flowing through the transmitter coil generates an electromagnetic field. This leads to induced voltages in the receiver coils. The amplitude of the receiving signal is spatially modulated using a conductive plate as counter part. Induced eddy currents in the conductive plate generate a secondary magnetic field which interacts with the primary field. This behavior is used to encode the angular position of the conductive plate. Therefore, either the coil structure or the conductive opponent has a static angular position, whereas the other one rotates. The drawback of this approach is the non-trivial design and implementation procedure. Contrary, it can be very robust against environmental effects such as moisture, oil contamination or dirt. To be retrofittable on rotating shafts the sensor geometry is limited to $270^\circ$. Same holds for the conductive plate which covers $180^\circ$. The modulated receiver signals are the basis for the angular position estimation which is performed by a dedicated transceiver chip. The transceiver is operated by a micro-controller which is further used for post-processing and to broadcast the gathered information on different interfaces. Wire-less communication using Bluetooth as well as Controller Area Network (CAN) bus connectivity is offered. The absolute error of the angular position estimate is smaller than $0.8^\circ$ under harsh conditions. Other systems based on magnetic principles achieve better accuracy, e.g. $< 0.2^\circ$ in [7], but have a $10\times$ lower bandwidth and lack retrofittability under limited space conditions. The applicability for industrial purposes is showcased using a forestry crane which executes a pick and place task of logs. To allow for autonomous acting of the crane, it requires feedback of it's joint states. Among

the crane joints, two rotary joints - one at it's base and one at it's end-effector, are of interest. The proposed sensor system is mounted on those joints without disassembling the crane. The rotary joints have different shaft diameters which is taken to demonstrate the scalability of the sensor front-end. Finally, the measured data is published to the CAN bus system offered by the industrial crane. Note, that the absolute error and update rate provided by the sensor are well in the specification limits of the industrial crane.

## II. System Description

A simple measurement model which if often used to determine the absolute angular position of a rotating part is formulated by

$$\mathbf{S}(\theta, \boldsymbol{\eta}) = \mathbf{A}(\boldsymbol{\eta}) \sin(\theta - \boldsymbol{\varphi}(\boldsymbol{\eta})) + \mathbf{w}, \tag{1}$$

where $\mathbf{S}(\theta, \boldsymbol{\eta})$ is the sensor output signal vector, $\theta$ represents the unknown angular position, $\boldsymbol{\varphi}(\boldsymbol{\eta})$ the phase shift of individual sensors and $\mathbf{A}(\boldsymbol{\eta})$ the amplitude vector. The measurement noise is modeled as multivariate additive white Gaussian noise $\mathbf{w} \sim \mathcal{N}(\mathbf{0}, \boldsymbol{\Sigma})$. A single observation, i.e. only one sensor, is not sufficient to estimate the absolute angular position using such a model. At least two different sensors are required. Throughout the paper two sensors are considered to keep the overall system complexity as low as possible. A natural lower bound of any unbiased estimator for the unknown parameters is obtained by the inverse Fisher Information [8]

$$\boldsymbol{\sigma}(\hat{\theta}) \geq \mathbf{I}(\theta, \boldsymbol{\eta})^{-1} \tag{2}$$

where $\boldsymbol{\sigma}(.)$ is the variance operator. A common goal of an optimal design procedure is to find a configuration that minimizes the lower bound, which is equivalent to a maximization of the Fisher Information $\mathbf{I}(\theta, \boldsymbol{\eta})$ of a sensor configuration. Using such a procedure the optimal angular displacement between the two used sensors can be determined. Therefore, (1) is rewritten as a I/Q model which yields

$$\mathbf{S}(\theta, \boldsymbol{\eta}) = I_A(\theta) \cos(\boldsymbol{\varphi}(\boldsymbol{\eta})) + Q_A(\theta) \sin(\boldsymbol{\varphi}(\boldsymbol{\eta})) + \mathbf{w}. \tag{3}$$

The goal is now to find the optimal sensor configuration assuming uncorrelated measurements. The Fisher Information is obtained as

$$\mathbf{I}(\theta) = \frac{1}{\sigma^2} \mathbf{H}^T \mathbf{H}, \tag{4}$$

where $\mathbf{H}$ is given as the spatial derivative of $\mathbf{S}(\theta, \boldsymbol{\eta})$. By computing the determinant of the Fisher Information for the two-sensor configuration we obtain the D-optimal design [9] as

$$\max \det(\mathbf{H}^T \mathbf{H}) = 1 - \cos(2\varphi_1 - 2\varphi_2) \tag{5}$$

which yields an optimal angular displacement of $\varphi_{opt} = \pi/2$ of the two sensor elements [10]. The estimate of the absolute angle can be obtained using the in-phase and quadrature contributions by computing the arctangent

$$\hat{\theta} = \text{atan2}(Q_A, I_A). \tag{6}$$

It is important to note, that the correct computation of the angle in (6) is only given if both contributions exhibit same amplitudes. In a practical situation this is not always true so that individual gain factors need to be introduced for an appropriate gain correction.

### A. Sensor Front-End Design

The sensor system proposed in this article is based on the mutual inductance between a transmitter and receiver coils. The transmitter coil carries a time varying sinusoidal signal which generates an electromagnetic field. The electromagnetic field induces a voltage in passive receiver coils. This field serves as a carrier which is spatially modulated. The modulation is achieved by shielding the magnetic field using a conductive plate. The electromagnetic field induces eddy currents in the conductive plate which generate a secondary magnetic field. The secondary field sums up with the primary field [11]. This fact, can be used to modulate the electromagnetic field depending on spatial constellations.

Generally, the induced voltage in any closed circuit [12] is given by

$$V = -\frac{d\Phi}{dt} = -\frac{d \int_{\mathbf{P}} \mu \mathbf{H} d\mathbf{A}}{dt}, \tag{7}$$

where $\Phi$ is the magnetic flux through the surface $\mathbf{P}$ enclosed by the circuit, $\mathbf{H}$ represents the magnetic field strength, $\mu$ represents the local permeability and $d\mathbf{A}$ is the infinitesimal surface element on $\mathbf{P}$. The target is to find a sensor geometry which sinusoidally modulates the amplitude of the magnetic flux through the receiver cross section, depending on the angular positon. Note, that the sensor is restricted in its design by the underlying geometry of any rotary shaft in order to be retrofittable. A typical application scenario is shown in Fig. 1. Here, a rotating shaft is connected to the non-rotating head.

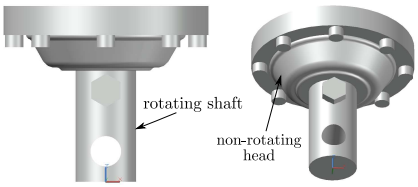


Fig. 1: A typical rotation shaft and its non-rotating counterpart is shown in profile and 3D view.

The angular position of the shaft with respect to the non-rotating head represents the target quantity. Clearly, a geometry which fully encircles the shaft is difficult to mount without disassembling the device. This paper introduces a structure which requires $270°$ space but is able to measure the absolute angular position of a full turn. The coils are flat coils printed on a Printed Circuit Board (PCB) on the non-rotating head of the shaft. The transmitter coil covers $270°$, whereas the passive coils cover $180°$ each and are located in the cross sectional area of the active coil as shown in Fig. 2. Since the optimal design is achieved by using two $90°$ phase shifted sensor elements, the receiver coils are orthogonal placed.

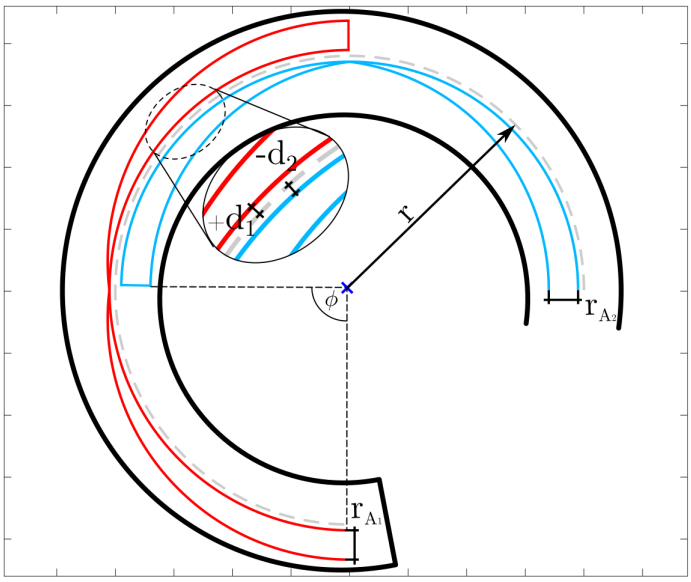


Fig. 2: Schematic view on the proposed coil design for the electromagnetic angular position sensor comprised by a single transmitter and two receivers. The transmitter coil is represented by the black line whereas the receivers are given by the red and blue lines.

The receiver coils cross sectional area $\mathbf{P}$ is given by

$$\mathbf{P} = \mathbf{A_C} - \mathbf{A_r}, \tag{8}$$

where $\mathbf{A_C}$ corresponds to the area under the modulated line $\mathbf{C}(\theta)$ given by the parametrization

$$\mathbf{C}(\theta) = \begin{bmatrix} (r + d + r_A|\sin(\theta)|) \cdot \cos(\theta + \phi) \\ (r + d + r_A|\sin(\theta)|) \cdot \sin(\theta + \phi) \end{bmatrix}. \tag{9}$$

The quantities $r$, $d$ and $r_A$ correspond the distances shown in Fig. 2. The angle $\phi$ is used to achieve the phase shift between the individual receivers. $\mathbf{A_r}$ is the area of a circular sector with radius $r + d$ and angle $\alpha = 180°$. The involved parameters are design parameters in a certain design space limited by factors such as shaft diameter, maximum size and minimum wire resolution of the PCB.

The conductive plate, denoted as $B$, is mounted on the rotating shaft and covers a half circle. It is placed closely on top of the sensor coils and covers them partly, depending on it's angular position. The resulting magnetic flux through the receiver coils can be calculated using Maxwell's equations. Therefore, suppose that the conductive plate $B$ is a bounded, smooth domain and let the constant quantities $\mu_\star$ and $\sigma_\star$ denote the permeability and the conductivity of $B$. The piecewise constant magnetic permeability and electric conductivity is given by

$$\mu_a = \begin{cases} \mu_\star & \text{in } B \\ \mu_0 & \text{in } B^c = \mathbb{R}^3 \setminus B \end{cases} \qquad \sigma_a = \begin{cases} \sigma_\star & \text{in } B \\ \sigma_0 & \text{in } B^c. \end{cases} \tag{10}$$

Let $(\mathbf{E}_a, \mathbf{H}_a)$ denote the eddy current fields in presence of the electromagnetic inclusion $B$ and a source current $\mathbf{J}_0$ located outside the inclusion. It is supposed that $\mathbf{J}_0$ is divergence free $\nabla \cdot \mathbf{J}_0 = 0$ in $\mathbb{R}^3$. The fields $(\mathbf{E}_a, \mathbf{H}_a)$ are the solutions of the following eddy current equations

$$\begin{cases} \nabla \times \mathbf{E}_a = i\omega\mu_a \mathbf{H}_a & \text{in } \mathbb{R}^3 \\ \nabla \times \mathbf{H}_a = \sigma_a \mathbf{E}_a + \mathbf{J}_0 & \text{in } \mathbb{R}^3 \\ \mathbf{E}_a(\mathbf{x}) = \mathcal{O}(|\mathbf{x}|^{-1}), \quad \mathbf{H}_a(\mathbf{x}) = \mathcal{O}(|\mathbf{x}|^{-1}) & \text{as } |\mathbf{x}| \to \infty. \end{cases} \tag{11}$$

A Finite Element Method (FEM) based simulation environments is further used to solve (11) for $\mathbf{H}_a$. The field solution is used to find appropriate coil design parameters. The first of the two receiver coils $R_1$ is optimized with respect to the introduced measurement model (1).

$$\begin{aligned} \underset{r, d_1, r_{A_1}}{\text{minimize}} \quad & \sum_{\theta=0}^{2\pi} (S(\theta, R_1) - |V_1(\theta, \mu_0, \mathbf{H}_a)|)^2 \\ \text{subject to} \quad & r, d_1, r_{A_1} \in \mathbf{D} \end{aligned} \tag{12}$$

Here, $S$ represents the measurement model, $|V_1(\theta, \mu_0, \mathbf{H}_a)|$ represents the amplitude of the voltage induced in the first receiver, $\mathbf{D}$ represents the geometric design space, e.g. shaft diameter and maximum PCB size, and $r, d_1, r_{A_1}$ are geometric design parameters as shown in Fig. 2. After designing the first receiver coil, the second coil can be designed by means of optimization with respect to the first coil.

$$\begin{aligned} \underset{d_2, r_{A_2}}{\text{minimize}} \quad & \sum_{\theta=0}^{2\pi} (\Phi_1 - \Phi_2)^2 \\ \text{subject to} \quad & d_2, r_{A_2} \in \mathbf{D} \end{aligned} \tag{13}$$

The difference in magnetic flux through the cross-section of the first coil, denoted as $\Phi_1$, and the second coil, denoted as $\Phi_2$, is minimized. This is equivalent to minimizing the difference in induced voltage. Note, that the 90° phase shift between the receivers is resolved before optimizing. Additionally, the receiver coil wires are crossed in their respective middle. Consequently, the net magnetic flux through their cross sections is zero for situations where the conductive plate completely covers the coil or does not cover it at all. The sinusoidal modulation oscillates around zero as a consequence. Detrimental situations such as tilt between the conductive plate and the coil structure can also be considered, e.g. by means of min-max optimization [13].

### B. System Back-End

The physical sensor interface is completed by a number of functional blocks. A schematic overview of the used blocks and their connections is shown in Fig. 3. In the following paragraph the functionality of each block is explained in detail. The transmitter coil and receiver coils, introduced in Section II-A, are efficiently driven using oscillator circuits. An external capacitor is used to achieve harmonic oscillations. The sinusoidal current flowing through the transmitter coil can then be generated using a rectangular driving signal. Additionally, capacitors are employed in the receiver circuit to account for higher receiving signals strengths. The received signals are sinusoidal shaped and moreover their amplitude is sinusoidal

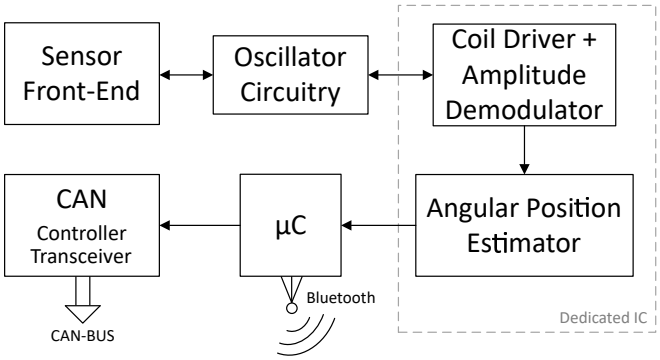


Fig. 3: A schematic overview showing the individual functional blocks of the angular position measurement system is reported.

modulated according to the magnetic field shielding effect described in Section II-A. The carrier is removed by means of amplitude demodulation and the result is a sinusoidal base-band signal per receiver. Note, that due to the orthogonal placement of the receiver coils a $90°$ phase shift between their base-band signals can be observed. They are further processed using (6), resulting in an estimate of the absolute angular position of the modulating conductive plate with respect to the coil geometry. Since, the plate is rigid mounted on the shaft, this also introduces information about the angular position of the rotating shaft. Typically, the coils can not be perfectly shaped and the conductive plate can not be ideally placed due to manufacturing limitations. Consequently, parasitic effects can be observed which lead to estimation errors. To decrease the influence of those effects a sensor calibration scheme is used. A look-up table containing the offsets between the model and the hardware realization at nine different angles is generated. The offset is used to correct the estimate at that specific angles. Angles between two calibration points are corrected by linear interpolation between the two offset values. The signal generator, the amplitude demodulation, the angle estimator as well as the calibration scheme is performed by a dedicated Integrated Circuit (IC), namely ZMID5201 by IDT. The output of the IC is an analog voltage representing the angular position estimate. This voltage is further sampled by an Analog-to-Digital Converter (ADC) provided by a micro-controller. The employed micro-controller is the NRF51822 by Nordic Semiconductor. Firstly, it is used to post-process the angle estimate and increase accuracy by further error correction as well as averaging over a number of samples. This is possible, because the update rate of the ZMID5201 IC is very high with respect to many applications in automation and robotics. Therefore, the update rate can be lowered without negative consequences but decreasing the variance of the estimate. The upper bound is given by $10\,\mathrm{kHz}$. Secondly, the micro-controller serves as interface to different communication channels. A printed $2.4\,\mathrm{GHz}$ antenna is connected to the micro-controller which is used for wireless communication, i.e. Bluetooth. More important for the log-crane application is the connectivity to CAN bus systems. Those bus systems can often be found in automation. Therefore, a dedicated CAN controller IC and a CAN transceiver IC called MSP2515 and MSP2551, respectively, are used. The published data can be used by e.g. a position controller of an autonomous system.

## III. Implementation

The applicability of the measurement system is showcased on the example of an hydraulic actuated industrial log-grasping crane. The crane is a 1:5 laboratory model of a crane employed at sawmills. It's total arm length is about $2.5\,\mathrm{m}$. The arm comes with two rotational joints, one at it's base and one at the end-effector. The rotational shafts of the different revolute joints have different diameters. However, the designed coils for one joint can be scaled to be applicable for the second joint. This fact makes the introduced design very flexible with respect to different sizes of rotation shafts. In the log-crane scenario the diameter of the base joint rotation shaft is $70\,\mathrm{mm}$ and the diameter of the end-effector rotation shaft is $40\,\mathrm{mm}$. The experimental implementation on the end-effector of the crane is shown in Fig. 4. Apart of it's size, the log-crane does not differ from a state-of-the-art real-world crane. Since those cranes are not meant to act autonomously, they are not equipped with sensors providing information about their internal states. Moreover, they are not thought to be equipped with retrofit sensor. Off-the-shelf sensor systems do not fit, because usable space for sensors is very limited which can also be seen in Fig. 4.

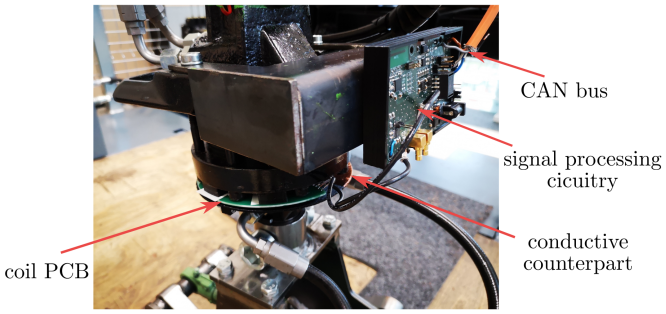


Fig. 4: The experimental sensor employment on the rotary joint of the end-effector is shown. The coil PCB is mounted to the non-rotating head whereas the conductive plate is mounted on the rotating shaft. The signal processing circuitry is also mounted on the non-rotating part. The conductive counterpart consists of a 3D printed holder and a copper foil wrapped around.

## IV. Results

The proposed sensor system is firstly verified in simulation and secondly experimentally implemented.

### A. Simulation Results

The simulation of the sensor system is based on a FEM simulation framework and is performed for two reasons. Firstly, the coil dimensions have to be determined as introduced in

(12) and (13). Secondly, the simulation is used to evaluate the performance of the found geometry. A simplified CAD model representing the log crane and the mounted sensor, shown in Fig. 5a, is used as simulation basis. The conductive plate and the coil wires are made of copper, the rotation shaft is made of steel and the PCB is made of FR-4. The excitation signal oscillates at $4.2\,\mathrm{MHz}$ with an amplitude of $1\,\mathrm{V}$. In contrast to the coil design shown in Fig. 2, the transmitter coil in simulation as well as in the experimental setup has several turns to increase the magnetic field strength. The underlying physical behaviour used in simulation is introduced in (11). Note, that the FEM mesh is extended until the field drops below the natural numerical boundary in order to avoid simulation border boundary conditions. Fig. 5b shows the magnetic flux density norm for a given constellation. The area where the conductive plate covers the coils results in less local magnetic field and induced voltage which is indicated as yellow area. Angular displacement of the conductive plate results in amplitude modulation in angular domain. After the

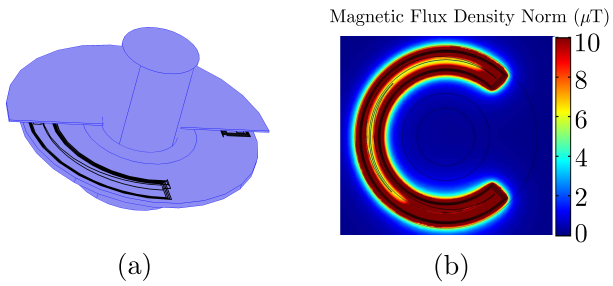


Fig. 5: Sub-plot (a) shows the simulated coil geometry including the rotating shaft, the coils and the conductive plate. Sub-plot (b) shows the absolute value of the magnetic flux density $\mathbf{B}$ for a given constellation.

coil design procedure a full rotation is performed and the amplitude of the induced voltage is used by the angle estimator (6). Note, that neither the calibration scheme nor any post-processing, e.g. averaging, is performed. The estimated angle as well as the ground-truth angle is reported in Fig. 6. It can be observed that the estimated angle is very accurate over the entire 360° range. This justifies the usage of the proposed coil design. However, various detrimental effects such as the metallic crane, moisture and oil contamination are not modelled. The robustness of the system with respect to the mentioned negative influences is shown in the experimental results.

### *B. Experimental Results*

The angular position measurement system including the calibration scheme is used as described in Fig. 3. The estimation result as well as the reference angle of a full turn is reported in Fig. 7. Despite, the improvements of the estimate due to the calibration significant errors remain. The main cause of those discrepancies is the mechanical construction of the conductive counterpart to the coils. Here, a 3D printed

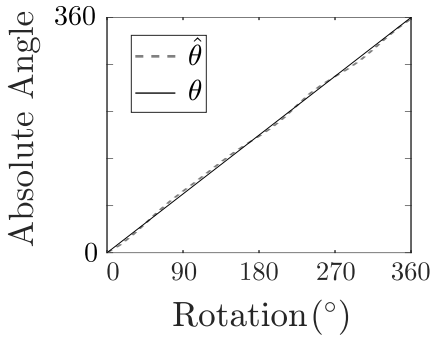


Fig. 6: The estimation result using the (6) estimator and the FEM based simulation data is shown. It can be observed, that the coil-design fits the needs of an angle estimator for sinusoidal signals.

holder with a copper foil wrapped around is used. The material used for the 3D printing is too flexible and the shape of the holder deforms when being mounted to the forestry crane. Note, that the curve can be fully corrected if it is strictly monotonic. Although, the results in Fig. 7 show non-strictly

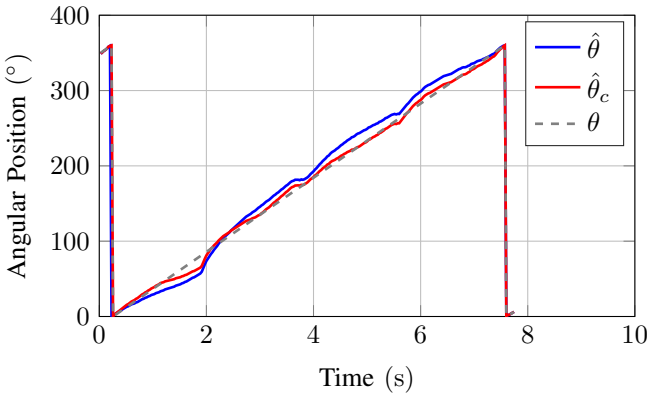


Fig. 7: The estimation result of the experimental setup is reported. Here, $\theta$ is the quantity to be estimated, i.e. the angular position of the forestry crane end-effector. $\hat{\theta}$ represents the estimated angle before calibration and $\hat{\theta}_c$ represents the angle estimate using the piece-wise linear sensor calibration function.

monotonic behaviour each quarter revolution. In fact, this occurs when one of the receiving coils is either fully or not at all covered by the conductive plate. To decrease this phenomena the conductive plate is increased in size to 184°. Therefore, linearity errors are introduced but contrary, most of the non-strictly monotonic points vanish. Subsequently, a full correction procedure, which provides a correction value to each sensory value to remove non-linearities, is performed on the micro-controller. The performance of the measurement system is evaluated in Fig. 8, which is based on several rotations of the crane end-effector. It can be observed, that the estimation result after the error correction stage is sufficiently accurate and stable over multiple turns.

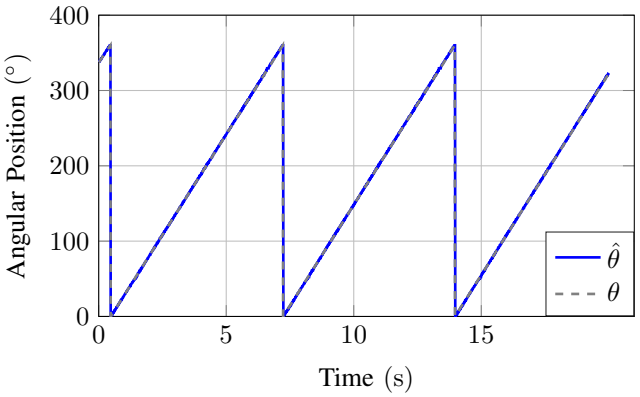


Fig. 8: Multiple turns of the log-crane end-effektor are performed and monitored by the proposed measurement system. Here, the dashed gray line $\theta$ represents the ground truth reference, whereas the estimation result is visualized as blue solid line $\hat{\theta}$.

Due to the hydraulic actuation of the crane accurate movement is denied. The smallest possible rotation of the end-effector is $1.5$ degree. The movement in Fig. 8 is performed at maximum angular velocity which is about $0.15\,\mathrm{Hz}$. At $329°$ a non-strictly monotonic point remains. It introduces an error of about $1.4°$ at $328° - 329°$. However, for the crane application this is not critical because of the small amplitude error and the predictable occurrence at a specific angle. For different applications it can further be optimized by resizing the conductive plate. Apart of this specific angular position the absolute error is smaller than $0.8$ degree. The maximum sensor update rate is $10\,\mathrm{kHz}$. However, in this application the measurement data is published to the CAN bus with $100\,\mathrm{Hz}$ which is sufficiently fast for the log-grasping scenario. The mean squared error over a full turn is given by $(0.55°)^2$. The experiment was repeated with the coils being contaminated with oil and water. The estimation result remained unchanged which substantiates the robustness of the sensor system. The robustness with respect to electromagnetic noise is not investigated at the current stage but is left open for future analysis. It can be summarized, that the sensor specifications, i.e. resolution, update-rate, accuracy, retrofittability and robustness, match the needs of an autonomous log-grasper as a representative for many industrial applications.

## V. Conclusion

This article presents an angular position measurement system, designed to match the needs of devices in the field of robotics and automation. Different applications in this domain operate under very harsh conditions, e.g. snow, moisture, dirt, bad illumination or vibration. The presented sensor front-end is comprised of a single transmitter and two receiver coils. The mutual inductance between transmitter and receiver coils is spatially modulated using conductive objects. The underlying physical principle serves for robustness with respect to many, often water- or oil-based, detrimental effects. The entire geometry requires $270°$ which makes it retrofittable to existing systems, e.g. mounting on a rotation shaft. The design of the sensor-fronted is automated by means of geometry optimization based on FEM simulation. Additionally, the sensor front-end is scalable in size to match different devices in automation. It's applicability is showcased on the example of a log-grasping crane featuring revolute joints with different sizes. The sensor provides an update rate up to $10\,\mathrm{kHz}$ with an absolute error smaller than $0.8$ degree under harsh conditions which is well in the specification limit of the log-crane.

## Acknowledgement

The research leading to these results has received funding from the Austrian Research Promotion Agency (FFG) under the grant agreement 864807 (Auto-LOG).

## References

[1] P. L. Fulmek, F. Wandling, W. Zdiarsky, G. Brasseur, and S. P. Cermak, "Capacitive sensor for relative angle measurement," *IEEE Transactions on Instrumentation and Measurement*, vol. 51, no. 6, pp. 1145–1149, Dec 2002.

[2] F. Cherchi, L. Disingrini, S. Gregori, G. Torelli, V. Liberali, and M. Gottardi, "A digital self-calibration circuit for optical rotary encoder microsystems," in *IMTC 2001. Proceedings of the 18th IEEE Instrumentation and Measurement Technology Conference. Rediscovering Measurement in the Age of Informatics (Cat. No.01CH 37188)*, vol. 3, May 2001, pp. 1619–1624 vol.3.

[3] A. Arami, J. D. Rechenmann, and K. Aminian, "Reference-free automated magnetic sensor calibration for angle estimation in smart knee prostheses," *IEEE Sensors Journal*, vol. 14, no. 6, pp. 1788–1796, June 2014.

[4] U. Ausserlechner, "The optimum layout for giant magneto-resistive angle sensors," *IEEE Sensors Journal*, vol. 10, no. 10, pp. 1571–1582, Oct 2010.

[5] H. Yamazaki, H. Hirabayashi, N. Oyama, and M. Sakai, "Characteristics of tmr angle sensors," in *Proceedings SENSOR 2011*, 2011, pp. 361–365.

[6] S. Wu, J. Chen, and S. Wu, "A rotary encoder with an eccentrically mounted ring magnet," *IEEE Transactions on Instrumentation and Measurement*, vol. 63, no. 8, pp. 1907–1915, Aug 2014.

[7] P. Kejik, S. Reymond, and R. S. Popovic, "Circular hall transducer for angular position sensing," in *TRANSDUCERS 2007 - 2007 International Solid-State Sensors, Actuators and Microsystems Conference*, June 2007, pp. 2593–2596.

[8] S. M. Kay, *Fundamentals of Statistical Signal Processing: Estimation Theory*. Prentice Hall, 1997.

[9] P. de Aguiar, B. Bourguignon, M. Khots, D. Massart, and R. Phan-Than-Luu, "D-optimal designs," *Chemometrics and Intelligent Laboratory Systems*, vol. 30, no. 2, pp. 199 – 210, 1995. [Online]. Available: http://www.sciencedirect.com/science/article/pii/016974399400076X

[10] H. Zangl, L.-M. Faller, and W. Granig, "Optimal design of angular position sensors," *COMPEL - The international journal for computation and mathematics in electrical and electronic engineering*, vol. 36, no. 5, pp. 1372–1385, 2017. [Online]. Available: https://doi.org/10.1108/COMPEL-02-2017-0099

[11] H. Gietler, H. Ammari, and H. Zangl, "Robust electromagnetic pose estimation for robotic applications," *IEEE Transactions on Instrumentation and Measurement*, pp. 1–12, 2019.

[12] J. D. Jackson, *Classical electrodynamics*, 3rd ed. New York, NY: Wiley, 1999. [Online]. Available: http://cdsweb.cern.ch/record/490457

[13] G. Heo, B. Schmuland, and D. P. Wiens, "Restricted minimax robust designs for misspecified regression models," *Canadian Journal of Statistics*, vol. 29, no. 1, pp. 117–128. [Online]. Available: https://onlinelibrary.wiley.com/doi/abs/10.2307/3316055